Optics Communications xxx (xxxx) xxx

Contents lists available at ScienceDirect

Optics Communications

journal homepage: www.elsevier.com/locate/optcom

High-speed and reliable Underwater Wireless Optical Communication system using Multiple-Input Multiple-Output and channel coding techniques for IoUT applications

Prasad Naik Ramavath *, Shripathi Acharya Udupi, Prabu Krishnan

Department of Electronics and Communication Engineering, National Institute of Technology Karnataka, Surathkal, Mangalore, 575025, India

ARTICLE INFO

Keywords:
Underwater Wireless Optical Communication (UWOC)
MIMO
RS-codes
Hyperbolic tangent distribution
Internet of Underwater Things (IoUT)

ABSTRACT

In this paper, we investigate the performance of an Underwater Wireless Optical Communication (UWOC) system employing on–off keying modulation at a data-rate of 500 Mbps over a link-range of 30 m. Transmit/receive diversity schemes, namely Multiple-Input to Single-Output (MISO), Single-Input to Multiple-Output (SIMO) and Multiple-Input to Multiple-Output (MIMO) techniques with and without RS-coding have been employed to mitigate the effects of weak oceanic turbulence and beam attenuation. The novel closed-form analytical Bit Error Rate (BER) expressions of Single-Input to Single-Output (SISO), SIMO, MISO and MIMO links for un-coded and RS-coded cases have been computed using the hyperbolic tangent distribution and validated with Monte-Carlo simulation results. The obtained BER results show that the use of (63, 51) RS-coded 4×5 MIMO UWOC system offers at-least 35 dB of transmit power gain compared with the un-coded SISO UWOC system at a BER of 10^{-5}. Emerging technologies like the fifth-generation (5G) networks and the Internet of Underwater Things (IoUT) will have a high impact on UWOC as these systems require a high degree of information integrity, high data rates and energy efficiency when employed in conjunction with data transfer between underwater vehicles and objects. The proposed RS-coded MIMO UWOC system offers high reliability and power efficiency and it has the potential to be gainfully employed in IoUT applications.

1. Introduction

In recent years, a number of researchers have turned their attention to the study, analysis and design of Underwater Wireless Optical Communication (UWOC) systems. This is because of the advantage of high transmission speeds and reliable communication over short ranges (~ tens of meters) in the ocean/seawater channels. This technology has the potential to enable many underwater services like ocean monitoring, safe navigation and disaster prevention, etc. The infrastructure to be put in place to enable these services has been referred to the Internet of Underwater Things (IoUT), which is a class of Internet of Things (IoT) and is defined as the network of smart underwater objects [1,2]. Recently, it has been proposed that underwater sensors can be interconnected with the data aggregating nodes through UWOC links to achieve high data-rate and reliability. The major limiting factors of the UWOC systems are beam absorption, scattering and underwater turbulence. Absorption reduces the intensity level and scattering causes deviation of the beam path away from the line of sight path directed towards the receiver. The combined effect of absorption and scattering will result in optical beam attenuation. The effect of attenuation can be minimized by the use of 400–530 nm wavelength LASER source [3,4].

The presence of underwater turbulence causes fluctuation of the light intensities from higher to lower levels, which degrades the system performance. A study of optical turbulence in underwater medium and corresponding BER performance is presented in [5]. It is well known that the effect of turbulence can be mitigated by the use of spatial diversity, optical amplification and channel coding techniques. Single-Input to Multiple-Output (SIMO) schemes such as maximum receiver combining, Equal Gain Combining (EGC) and selection combining have been employed to mitigate the effect of turbulence in UWOC systems [6]. It has been demonstrated that the performance of the EGC scheme is superior to all other schemes in the turbulent underwater medium [6]. The performance improvement obtained by the use of the EGC scheme along with the optical amplifier is proposed in [7]. The performance of the UWOC system can be further improved by employing multiple transmit sources along with the multiple detectors at the receiver discussed in [8].

The contributions of this paper are as follows. The Bit Error Rate (BER) performance of an On-Off Keying (OOK) modulation based UWOC system in weak turbulence and propagation loss due to beam attenuation regimes are studied for Single-Input to Single-Output (SISO),

* Corresponding author.
E-mail addresses: prasadnaikr@gmail.com (Prasad Naik R), sripati.acharya1@gmail.com (U. Shripathi Acharya), nitprabu@gmail.com (Prabu K).

https://doi.org/10.1016/j.optcom.2019.125229
Received 14 October 2019; Received in revised form 14 December 2019; Accepted 31 December 2019
Available online xxxx
0030-4018/

Please cite this article as: Prasad Naik R, U. Shripathi Acharya and Prabu K, High-speed and reliable Underwater Wireless Optical Communication system using Multiple-Input Multiple-Output and channel coding techniques for IoUT applications, Optics Communications (2020) 125229, https://doi.org/10.1016/j.optcom.2019.125229.

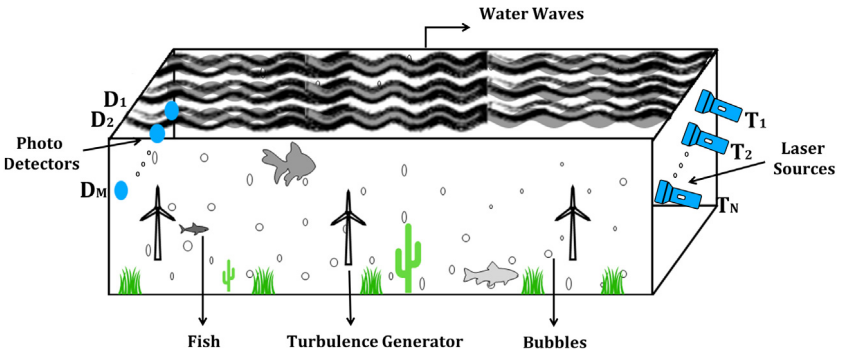

Fig. 1. Schematic diagram of a UWOC system.

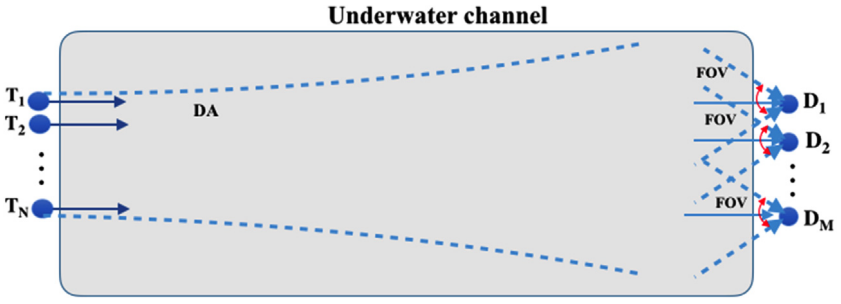

Fig. 2. Link geometry of MIMO UWOC system.

Single-Input to Multiple-Output (SIMO), Multiple-Input to Single-Output (MISO) and Multiple-Input to Multiple-Output (MIMO) schemes. The performance of the links in the presence of (63, 51) RS-code is determined and compared with the un-coded system performance. This RS-code is chosen because of its moderate complexity and ability to correct burst errors [9]. The transmission speed is fixed at 500 Mbps and the link range is set to 30 m. The analytical closed-form expressions for the BER are derived by use of the Hyperbolic Tangent Distribution (HTD) family to validate the Monte-Carlo simulation results. Throughout this paper, the performance improvement is defined in terms of 'transmit power gain', which is the reduction in transmit power observed to obtain a BER of 10^{-5} when the two competing schemes are used.

The remaining part of the paper is organized as follows. Section 2 describes the system and UWOC channel model. RS-code encoding and decoding are presented in Section 3. A closed-form expression for the BER pertaining to the UWOC system employing different diversity and MIMO techniques for un-coded and RS-coded cases are presented in Section 4. Monte-Carlo simulation and analytical results specifying the BER as a function of transmit power are provided in Section 5. The paper is concluded in Section 6 with a brief discussion of the analytic and simulation results obtained and their significance.

2. System and channel model

The system and channel models of a UWOC link operating under the influence of weak oceanic turbulence and beam attenuation scenarios are presented in this section.

2.1. System model

Consider an OOK modulated UWOC system with N number of LASER sources (λ = 470 nm wavelength) at the transmitter and M number of Photo-Detectors (PD) at the receiver. The same data is transmitted from all the sources and the data symbols received by M detectors are combined using EGC. Fig. 1, depicts the UWOC system schematic diagram, where $T_1, T_2, \ldots, T_N$ are N number of LASER

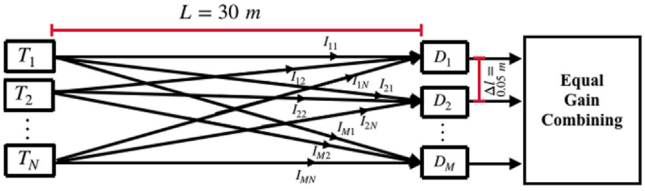

Fig. 3. Structure of transmit and receive array.

sources and $D_1, D_2, \ldots, D_M$ are M PDs. We have considered the MIMO UWOC system with the transmit and receiver array separated by 30 m far and facing each other. A separation of 5 cm between adjacent LASER sources at the transmitter and PDs at the receiver is maintained. The LASER sources and PD modules are assumed to be in the line of sight and the Divergence Angle (DA) of LASER sources is with in the Field Of View (FOV) of all available PDs. Figs. 2 and 3 are shows the link geometry and structure of the MIMO UWOC transmitter and receiver array.

It is considered that a binary '1' is communicated with P_t watts of optical power (amplitude across individual source is $A = \sqrt{P_t T_b / N}$ among N available sources) and binary '0' is communicated with 0 watts of optical power (amplitude $A = 0$) for a duration of T_b s (Conventional OOK modulated system) through the N sources. The received symbol at the i^{th} PD can be expressed as [10],

$$Y_i = \eta_i A \left(\sum_{j=1}^{N} I_{ij} \right) s + n_i = \eta_i \sqrt{\frac{P_t T_b}{N}} \left(\sum_{j=1}^{N} I_{ij} \right) s + n_i, \quad 1 \le i \le M \qquad (1)$$

where Y_i represents the response of i^{th} PD after trans-impedance amplification and it is represented in terms of volts, P_t is transmit power per bit (mW), $s \in (0, 1)$ represents the information bits, η_i represents detector's responsivity (A/W), I_{ij} is irradiance received from j^{th} source to i^{th} detector and channel noise n_i is the additive white Gaussian noise with zero mean and variance σ^2. Here, we have assumed the source of noise variance to be thermal noise only and ignored the noise variance due to background and shot noise (due to these noise

Please cite this article as: Prasad Naik R, U. Shripathi Acharya and Prabu K, High-speed and reliable Underwater Wireless Optical Communication system using Multiple-Input Multiple-Output and channel coding techniques for IoUT applications, Optics Communications (2020) 125229, https://doi.org/10.1016/j.optcom.2019.125229.

variances being significantly smaller than the variance of thermal noise source). Thus, noise variance is specified as $\sigma^2 = 4K_bT_eB/R_L$, where $K_b = 1.38 \times 10^{-23}$ J/K is the Boltzmann's constant, $T_e = 256$ K is the absolute receiver temperature, $B = 2$ GHz is electronic bandwidth, $R_L = 100\ \Omega$ is load resistance of the detector, which leads the noise variance $\sigma^2 = 2.82 \times 10^{-13}$ [11].

2.2. Channel model

In this section, we present the distribution of the UWOC channel in the presence of weak turbulence and beam attenuation scenarios.

2.2.1. Attenuation channel model

UWOC channel exhibits beam attenuation due to absorption and scattering. Beam attenuation in UWOC channel is deterministic in nature and it can be determined by use of Beer–Lambert's law, which is given as [12],

$$I_a = \exp\left(-C(\lambda)L\right) \tag{2}$$

where $C(\lambda) = A(\lambda) + B(\lambda)$ is attenuation coefficient, $A(\lambda)$ and $B(\lambda)$ are absorption and scattering coefficients respectively and these values changes with the different wavelength sources and different water types.

2.2.2. Turbulence channel model

Turbulence due to movement of water medium can fluctuate the optical signal strength. The irradiance (I_t) fluctuation due to underwater weak turbulence is characterized by log-normal density function [13,14]. The Probability Density Function (PDF) of a log-normally distributed random variable I is given by,

$$f_{I_t}(I_t) = \frac{1}{2I_t}\frac{1}{\sqrt{2\pi\sigma_X^2}} exp\left(-\frac{\left(ln(I_t) - 2\mu_X\right)^2}{8\sigma_X^2}\right) \tag{3}$$

where μ_X and σ_X^2 are mean and variance respectively of the Gaussian distributed random variable $X = \ln(I_t)/2$. Normalized log-normal PDF can be obtained by considering $\mathbb{E}(I_t) = 1$, which implies $\mu_X = -\sigma_X^2$ and Gaussian variance $\sigma_X^2 = 0.25\ln\left(\sigma_{I_t}^2 + 1\right)$, where $\mathbb{E}(\cdot)$ denotes expectation, $\sigma_{I_t}^2$ is Scintillation Index (SI). The SI for plane wave in the presence of underwater turbulence is given as [15,16],

$$\sigma_{I_t}^2 = 8\pi^2k^2L\int_0^1\int_0^\infty \mathcal{K}\Phi_n(\mathcal{K})\left(1 - \cos\left(\frac{L\mathscr{L}\mathcal{K}^2}{k}\right)\right)d\mathcal{K}d\mathscr{L} \tag{4}$$

where $k = 2\pi/\lambda$ is the wave-number, λ is the wavelength of the LASER source, L is link-range, $\Phi_n(\mathcal{K})$ is power spectrum of oceanic water and it is given as [16],

$$\Phi_n(\mathcal{K}) = \frac{0.388 \times 10^{-8}\epsilon^{-1/3}\mathcal{K}^{-11/3}\chi_T}{\omega^2}\left[1 + 2.35\left(\mathcal{K}\xi\right)^{2/3}\right] \times \left(\omega^2 e^{-A_T\delta} + e^{-A_S\delta} - 2\omega e^{-A_{TS}\delta}\right) \tag{5}$$

where Kolmogorov micro-scale length $\xi = 10^{-3}$ m, ϵ is rate of dissipation of turbulent kinetic energy per unit mass (m^2/s^3), χ_T is the dissipation rate of mean square temperature (K^2/s) and ω is a unitless quantity that represents the strength of the temperature–salinity parameter, respectively. The values of ω in the range of $[-5, 0]$, $\omega = -5$ corresponds to temperature dominant turbulence, $\omega = 0$ corresponds to salinity dominant turbulence and minus sign indicates that a reduction in temperature and an increase in salinity with depth [17]. The remaining parameters A_T, A_S, A_{TS} and δ are considered as specified in [16].

2.2.3. Combined channel model

The channel gain due to the combined effect of underwater turbulence and propagation loss due to attenuation is $I = I_tI_a$ and corresponding PDF is obtained as,

$$f_I(I) = \frac{1}{2I\sqrt{2\pi\sigma_X^2}}\exp\left(-\frac{\left(\ln(I/I_a) - 2\mu_X\right)^2}{8\sigma_X^2}\right) \tag{6}$$

3. Reed-solomon coding and decoding

In underwater channels, the data transmission can be occasionally blocked for certain durations due to the movement of large water mammals or schools of fish. During this duration, the transmission path could be entirely blocked due to which burst or random error is induced in the information stream. Channel codes can correct random or burst errors. Turbo codes and Low-Density Parity-Check codes (LDPC) are efficient random error-correcting codes, whereas RS-codes possess excellent burst error-correcting capability [18,19]. In UWOC systems, the probability of encountering burst errors is high. Hence, we have proposed the use of RS-codes in UWOC systems to improve the integrity of information transmission. The procedure of RS-code encoding and decoding is provided in Section 3.1.

3.1. Encoding and decoding of $(n,\ k,\ t)$ RS-codes

The generator polynomial of an n-length RS-code over Galois Field $GF(q)$, $(q = p^m$, p is a prime number, m is the order of the field extension and $n|\ (p^m - 1))$ with t symbol error correcting capability is defined by, $g(x) = (x - \alpha^b)(x - \alpha^{b+1})\ldots(x - \alpha^{b+\delta-2})$, where α is a primitive element of the $GF(p^m)$, $b \geq 0$ is any real positive integer and $\delta = 2t + 1$. The generator polynomial of $(n,\ k)$ RS-code with $b = 1$ (typical choice) and t symbol error correcting capability can be expressed as [18],

$$g(x) = (x - \alpha)(x - \alpha^2)\ldots(x - \alpha^{2t-1})(x - \alpha^{2t}) \tag{7}$$

where all the computations are performed in the field $GF(p^m)$. The code-word polynomial is defined by $c(x) = g(x) \times s(x)$, where $g(x)$ is the generator polynomial and $s(x) = s_0 + s_1x + s_2x^2 + \cdots + s_{k-1}x^{k-1}$ is the message polynomial obtained by representing the k message symbols $s_0, s_1, s_2, \ldots, s_{k-1}$ as a polynomial in the indeterminate x. The $n-$ length code-word is represented in polynomial form as $c(x) = c_0 + c_1x + c_2x^2 + \cdots + c_{n-1}x^{n-1}$ and bears one to one correspondence to the information bearing (message) polynomial $s(x) = s_0 + s_1x + s_2x^2 + \cdots + s_{k-1}x^{k-1}$. In this paper, a $(n = 63,\ k = 51)$ RS code over the field $GF(2^6)$ has been designed and employed for error detection/correction. Each symbol from the field $GF(2^6)$ can be expressed as a binary 6-tuple. Each individual symbol of the code-word polynomial is converted into 6-tuple of binary bits and communicated through the UWOC channel via an OOK modulated LASER source. At the receiver, the incoming bits are combined into 6 bit symbols lying in the field $GF(2^6)$. A set of successive 63 6-bit symbols constitutes the received vector $r(x) = r_{(0)} + r_{(1)}x + r_{(2)}x^2 + \cdots + r_{(n-1)}x^{n-1}$, where $r_{(i)}$ represents the extracted ith symbol, $i = 0, 1, \ldots, n-1$, which is then processed to determine the error locations and error magnitudes. Berlekamp–Massey algorithm and Chien search algorithm are employed for determining the locations in which the channel has induced errors and Forney's algorithm is used to determine the error magnitudes. The estimate of transmitted code-word is then determined by $\hat{c}(x) = r(x) - e(x)$, where $e(x) = \sum_{i=0}^{n-1} e_ix^i$, e_i is the ith error magnitude obtained by the use of Forney's algorithm and x^i represents the ith error location obtained by making use of Berlekamp–Massey and Chien search algorithms.

4. Analytical BER evaluation

A closed-form BER expression corresponding to the use of SISO, SIMO, MISO and MIMO schemes for un-coded and RS-coded cases has been evaluated in this section.

4.1. Single-input single-output

The received OOK modulated symbol in the presence of combined underwater channel is given as,

$$Y = \eta I\sqrt{P_tT_b}s + n \tag{8}$$

Please cite this article as: Prasad Naik R, U. Shripathi Acharya and Prabu K, High-speed and reliable Underwater Wireless Optical Communication system using Multiple-Input Multiple-Output and channel coding techniques for IoUT applications, Optics Communications (2020) 125229, https://doi.org/10.1016/j.optcom.2019.125229.

The BER of SISO (P_{siso}) with equiprobable input bits (assuming known log-normally distributed channel) is specified by,

$$P_{siso} = \frac{1}{2}\int_0^\infty \left(P\left(\frac{\hat{s}=1}{s=0,I}\right) + P\left(\frac{\hat{s}=0}{s=1,I}\right)\right) f_I(I)dI \tag{9}$$

where, $P_0 = P\left(\frac{\hat{s}=1}{s=0,I}\right)$ is the probability of estimated data being inferred as '1' when transmitted data is '0', $P_1 = P\left(\frac{\hat{s}=0}{s=1,I}\right)$ is the probability of estimated data being inferred as '0' when transmitted data is '1' and $f_I(I)$ is log-normal density function. The BER of SISO by setting the threshold equal to $\eta I\sqrt{P_tT_b}/2$ between the received levels corresponding the two binary symbols and substituting Eq. (3) in Eq. (9) is,

$$P_{siso} = \int_0^\infty \mathbb{Q}\left(\eta I\sqrt{\frac{P_tT_b}{4\sigma^2}}\right)\frac{1}{2I}\frac{1}{\sqrt{2\pi\sigma_X^2}}exp\left(-\frac{\left(ln(I/I_a)-2\mu_X\right)^2}{8\sigma_X^2}\right)dI \tag{10}$$

where $\mathbb{Q}(x) \triangleq (1/\sqrt{2\pi})\int_x^\infty \exp(-y^2/2)dy$ is Gaussian Q-function. Substituting $I/I_a = t$ in Eq. (10), the obtained equation is given as,

$$P_{siso} = \int_0^\infty \mathbb{Q}\left(\eta I_a t\sqrt{\frac{P_tT_b}{4\sigma^2}}\right)\frac{1}{2t}\frac{1}{\sqrt{2\pi\sigma_X^2}}exp\left(-\frac{\left(ln(t)-2\mu_X\right)^2}{8\sigma_X^2}\right)dt \tag{11}$$

Solution for Eq. (11) does not exist [20], closed-form solutions can be obtained by use of Gauss–Hermite Quadrature [20] and power series method proposed in [21]. In this paper, to facilitate the determination of closed-form solutions, we have used the Hyperbolic Tangent Distribution (HTD) family to specify the log-normal PDF in algebraic form, so that the solution to Eq. (11) can be obtained and the BER results obtained by employing HTD has fair match with the simulations obtained by Monte-Carlo. The log-normal PDF representation using the HTD family given in Appendix A. By substituting log-normal PDF generated by HTD in Eq. (11), the reformulated equation is given as,

$$P_{siso} \approx \int_0^\infty \left(\frac{1}{12}\exp\left(-\frac{\zeta^2t^2}{2}\right)+\frac{1}{4}\exp\left(-\frac{2\zeta^2t^2}{3}\right)\right) \times\left(\frac{b\exp(2a)t^{b-1}}{\left(1+\exp(2a)\,t^b\right)^2}\right)dt \tag{12}$$

where $\zeta = \eta I_a\sqrt{\frac{P_tT_b}{4\sigma^2}}$, $\mathbb{Q}(x)$ is approximated using [22] as $\mathbb{Q}(x) \approx 1/12\exp\left(-x^2/2\right)+1/4\exp\left(-2x^2/3\right)$, a and b are obtained from HTD family for a particular mean and variance of normal density function (i.e, μ_X and σ_X^2) given in Table 3. The closed-form expression is obtained by substitution and then integration of Eq. 12 using Eq. (21) of [23] and the obtained expression is given as,

$$P_{siso} \approx 2\exp(2a)\left(\frac{b}{2\pi}\right)^{\frac{b+1}{2}}\left[\frac{\mathscr{C}_1}{12}+\frac{\mathscr{C}_2}{4}\right] \tag{13}$$

where $\mathscr{C}_1 = \left(\sqrt{2}/\zeta\right)^b G^{2,2+b}_{2+b,2}\left(\begin{matrix}-\frac{1}{2},0,\frac{i-\frac{b}{2}}{b}\\ 0,\frac{1}{2}\end{matrix}\middle| b^b\mathscr{P}_1^2\right)$, $\mathscr{C}_2 = \left(\sqrt{1.5}/\zeta\right)^b G^{2,2+b}_{2+b,2}\left(\begin{matrix}-\frac{1}{2},0,\frac{i-\frac{b}{2}}{b}\\ 0,\frac{1}{2}\end{matrix}\middle| b^b\mathscr{P}_2^2\right)$, $i = 1,2,\ldots,b$; $\mathscr{P}_1 = \exp(2a)\left(\sqrt{2}/\zeta\right)^b$, $\mathscr{P}_2 = \exp(2a)\left(\sqrt{1.5}/\zeta\right)^b$ and $G[\cdot]$ is Meijer G-function.

4.2. Single-input multiple-output

It is assumed that a LASER source transmits data through the UWOC channel and SIMO scheme averages (EGC) the response produced by all individual detectors. The average of the combined response produced by M detectors is $Y = \frac{\eta\sqrt{P_tT_b}sI_mI_a}{M} + n$, where $I_m = \sum_{i=0}^{M} I_i$ and I_i's are independent log-normal random variables with identical mean and variances. The sum of M independent log-normal random variables having identical mean and variance is also a log-normally distributed random variable [24]. Hence, $I_m = \exp(2\mathscr{M})$ is also a log-normally distributed random variable, where $\mathscr{M}$ is normal random variable with mean μ_m and variance σ_m^2 (mean and variance of $\mathscr{M}$ given in Appendix B). The density function of the sum of M log-normal random variables is given as,

$$f_{I_m}(I_m) = \frac{1}{2I_m\sqrt{2\pi\sigma_m^2}}\exp\left(-\frac{\left(\ln(I_m)-2\mu_m\right)^2}{8\sigma_m^2}\right) \tag{14}$$

where, $\mu_m = \frac{1}{2}\ln(M) - \frac{1}{4}\ln\left(1+\frac{\exp\left(4\sigma_X^2\right)-1}{M}\right)$ and $\sigma_m^2 = \frac{1}{4}\ln\left(1+\frac{\exp\left(4\sigma_X^2\right)-1}{M}\right)$ are mean and variance of normal random variable $\mathscr{M}$. The BER associated with SIMO system is given as,

$$P_{simo} = \int_0^\infty \mathbb{Q}\left(\zeta\frac{I_m}{M}\right) f_{I_m}(I_m)dI_m \tag{15}$$

Eq. (15) is also computed in a similar manner to Eq. (12). The analytical BER obtained as,

$$P_{simo} \approx 2\exp(2a)\left(\frac{b}{2\pi}\right)^{\frac{b+1}{2}}\left[\frac{\mathscr{D}_1}{12}+\frac{\mathscr{D}_2}{4}\right] \tag{16}$$

where $\mathscr{D}_1 = \left(\sqrt{2}M/\zeta\right)^b G^{2,2+b}_{2+b,2}\left(\begin{matrix}-\frac{1}{2},0,\frac{i-\frac{b}{2}}{b}\\ 0,\frac{1}{2}\end{matrix}\middle| b^b\mathscr{R}_1^2\right)$, $\mathscr{D}_2 = \left(\sqrt{1.5}M/\zeta\right)^b G^{2,2+b}_{2+b,2}\left(\begin{matrix}-\frac{1}{2},0,\frac{i-\frac{b}{2}}{b}\\ 0,\frac{1}{2}\end{matrix}\middle| b^b\mathscr{R}_2^2\right)$, $i = 1,2,\ldots,b$; $\mathscr{R}_1 = \exp(2a)\left(\sqrt{2}M/\zeta\right)^b$, $\mathscr{R}_2 = \exp(2a)\left(\sqrt{1.5}M/\zeta\right)^b$, a and b values for various M (μ_m and σ_m^2 varies with M) are given in Table 3.

4.3. Multiple-input single-output

Assume that N transmit sources transmit the same data through the underwater channel and the detector's response is $Y = \eta I_aI_n\sqrt{(P_tT_b/N)}s + n$ where $I_n = I_1+I_2+\cdots+I_N$, since I_i's are log-normal random variables then $I_n = \exp(2\mathscr{N})$ is also log-normal random variable and $\mathscr{N}$ is normal random variable with mean $\mu_n = \frac{1}{2}\ln(N) - \frac{1}{4}\ln\left(1+\frac{\exp\left(4\sigma_X^2\right)-1}{N}\right)$ and variance $\sigma_n^2 = \frac{1}{4}\ln\left(1+\frac{\exp\left(4\sigma_X^2\right)-1}{N}\right)$. The BER of MISO system is given as,

$$P_{miso} = \int_0^\infty \mathbb{Q}\left(\frac{\zeta I_n}{\sqrt{N}}\right) f_{I_n}(I_n)dI \tag{17}$$

where $f_{I_n}(I_n)$ is log-normal PDF and it is obtained into algebraic form using HTD. The simplified BER equation can be obtained by solving similar way of BER of SISO and it is given as,

$$P_{miso} \approx 2\exp(2a)\left(\frac{b}{2\pi}\right)^{\frac{b+1}{2}}\left[\frac{\mathscr{C}_1}{12}+\frac{\mathscr{C}_2}{4}\right] \tag{18}$$

where $\mathscr{C}_1 = \left(\sqrt{2N}/\zeta\right)^b G^{2,2+b}_{2+b,2}\left(\begin{matrix}-\frac{1}{2},0,\frac{i-\frac{b}{2}}{b}\\ 0,\frac{1}{2}\end{matrix}\middle| b^b\mathscr{P}_1^2\right)$, $\mathscr{C}_2 = \left(\sqrt{1.5N}/\zeta\right)^b G^{2,2+b}_{2+b,2}\left(\begin{matrix}-\frac{1}{2},0,\frac{i-\frac{b}{2}}{b}\\ 0,\frac{1}{2}\end{matrix}\middle| b^b\mathscr{P}_2^2\right)$, $\mathscr{P}_1$, $\mathscr{P}_2$ are given under Eq. (13), the variation in a and b values with respect μ_n and σ_n^2 of particular N is given in Table 3.

4.4. Multiple-input multiple-output

Multiple transmit sources T_1, T_2, …, T_N are used to transmit same information through the channel and the detector's responses are combined using EGC at the receiver. The combined response is $Y = \sum_{i=1}^{M}\frac{Y_i}{M}$,

Please cite this article as: Prasad Naik R, U. Shripathi Acharya and Prabu K, High-speed and reliable Underwater Wireless Optical Communication system using Multiple-Input Multiple-Output and channel coding techniques for IoUT applications, Optics Communications (2020) 125229, https://doi.org/10.1016/j.optcom.2019.125229.

where $Y_i = \eta I_a \left(\sum_{j=1}^{N} I_{ij}\right) \sqrt{P_t T_b} s + n$, $I_{11}, \ldots, I_{MN}$ are independent log-normal random variables, the resultant summation ($I_{mn} = \exp(\mathscr{O})$) is also a log-normal random variable, where $\mathscr{O}$ is a normally distributed random variable with mean $\mu_{mn} = \frac{1}{2}\ln(MN) - \frac{1}{4}\ln\left(1 + \frac{\exp\left(4\sigma_X^2\right)-1}{MN}\right)$ and variance $\sigma_{mn}^2 = \frac{1}{4}\ln\left(1 + \frac{\exp\left(4\sigma_X^2\right)-1}{MN}\right)$. The probability of error associated with this MIMO scheme can be expressed as,

$$P_{mimo} = \int_0^{\infty} \mathbb{Q}\left(\frac{\zeta I_{mn}}{M\sqrt{N}}\right) f_{I_{mn}}(I_{mn}) d I_{mn} \tag{19}$$

where $I_{mn} = I_{11} + I_{12} + \cdots + I_{MN}$ and $f_{I_{mn}}(I_{mn})$ is PDF of log-normal random variable I_{mn}. Similar to Eq. (16), the closed-form solution is,

$$P_{mimo} \approx 2\exp(2a)\left(\frac{b}{2\pi}\right)^{\frac{b+1}{2}} \left[\frac{\mathscr{D}_1}{12} + \frac{\mathscr{D}_2}{4}\right] \tag{20}$$

where $\mathscr{D}_1 = \left(M\sqrt{2N}/\zeta\right)^b G_{2+b,2}^{2,2+b}\left(\begin{matrix} -\frac{1}{2}, 0, \frac{i-\frac{b}{2}}{b} \\ 0, \frac{1}{2} \end{matrix} \middle| b^b \mathscr{R}_1^2\right)$, $\mathscr{D}_2 = \left(M\sqrt{1.5N}/\zeta\right)^b G_{2+b,2}^{2,2+b}\left(\begin{matrix} -\frac{1}{2}, 0, \frac{i-\frac{b}{2}}{b} \\ 0, \frac{1}{2} \end{matrix} \middle| b^b \mathscr{R}_2^2\right)$, $i = 1, 2, \ldots, b$; $\mathscr{R}_1$, $\mathscr{R}_2$ are given under Eq. (16) and the values of a and b are given in Table 3 for different M and N values.

4.5. Coded BER evaluation

When the decoded code-word is not identical to the transmitted code-word, a decoding error is said to occur. An upper bound on the BER (P_d) associated with a (n, k, t) non-binary RS-code over $GF(2^m)$ with t symbol error correcting capability and symbol error probability P_s is given by [25],

$$P_d \leq \sum_{i=t+1}^{n} \binom{n}{i} P_s^i \left(1 - P_s\right)^{n-i} \tag{21}$$

where $P_s = 1 - (1 - p_b)^m$, p_b represents the transition probability of the binary symmetric channel. In the presented analysis, p_b corresponds to P_{siso} in Eq. (13), P_{simo} in Eq. (16), P_{miso} in Eq. (18) and P_{mimo} in Eq. (20) for SISO, SIMO, MISO and MIMO schemes respectively with code-rate $r = k/n$.

5. Results and discussions

In this section, we present the simulation and analytical BER results of the OOK modulated UWOC system as a function of transmit power per bit in dB.

The simulations of the BER of the UWOC system are based on the transmission of $l = 10^6$ binary data bits (s) generated using a pseudo-random binary generator. Each data sample drives a N number of laser sources in parallel. The irradiance produced by the laser sources is then communicated through the UWOC channel. The irradiance values received by the M detectors are processed to determine the estimate of the communicated data bit ($\hat{s}$). The BER is computed as $\sum_i^l (s_i \oplus \hat{s}_i)/l$ for varying transmit powers, where $\oplus$ denotes exclusive-or operation. Analytical BER results are determined based on the Eqs. (13), (16), (18) and (20) derived in this paper. All these equations are as a function of transmit powers, so the analytical BER results obtained by varying the transmit powers in the obtained equations.

The system parameters used in simulation and computation are $\eta = 0.8$ A/W, data-rate $R_b = 500$ Mbps, bit duration $T_b = 1/R_b = 2$ ns and link-range $L = 30$ m. The parameters used for calculation of scintillation index for plane wave propagating in water are $\omega = -2.5$, $\chi_t = 5.84 \times 10^{-5}$ K^2/s and $\epsilon = 1 \times 10^{-5}$ m^2/s^3 and remaining parameters are the same values as in [16]. These values substituted in Eq. (4) yields $\sigma_I^2 = 0.9328$ and $\sigma_X^2 = 0.1647$. The attenuation coefficient considered for evaluating system behavior in the presence of beam attenuation is $C(\lambda = 470\text{ nm}) = 0.1514$ m^{-1} for clear ocean water as given in [26].

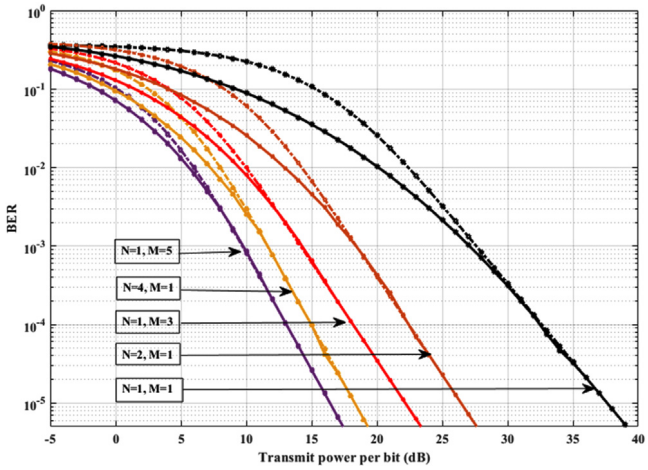

Fig. 4. Simulation and analytical BER results of SISO, SIMO and MISO UWOC system.

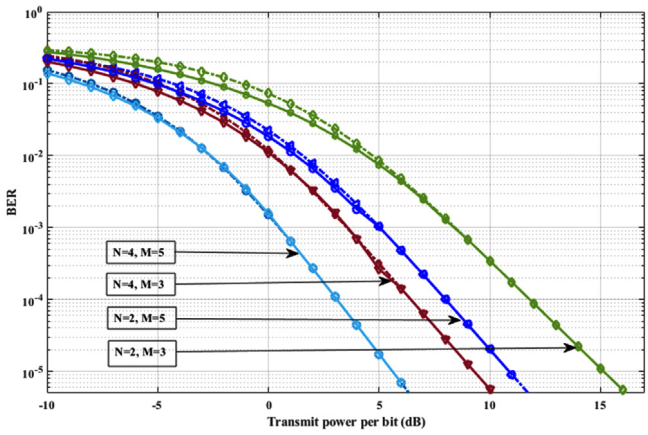

Fig. 5. Simulation and analytical BER results of MIMO UWOC system.

In [26], Hanson et al. have determined the attenuation coefficient for 514 nm wavelength source, which is approximately the same for 470 nm source.

Figs. 4 and 5 illustrates the variation of the BER simulation values (solid lines) and analytic values (dash and dot line) for an UWOC system for SISO, SIMO, MISO and MIMO configurations. An examination of Figs. 4 and 5 show that the analytical results are close correspondence with the obtained simulation results and the BER performance improves with increasing M and N. For $N = 2$ and 4 MISO systems, a performance improvement of 11 dB and 19.3 dB respectively from SISO at a BER of 10^{-5} is observed. For SIMO schemes employing $M = 3$ and 5, a performance improvement of 15.5 dB ($M = 3$) and 21.2 dB ($M = 5$) is observed when compared with SISO UWOC system at a BER of 10^{-5}. From Fig. 5, an improvement in performance of nearly $3 - 4$ dB is observed when we move from $N \times 3$ MIMO to $N \times 5$ MIMO for $N = 2, 4$. Further, a performance improvement of nearly 5–6 dB is observed when we move from $2 \times M$ to $4 \times M$ for $M = 3, 5$ at BER of 10^{-5}.

From Figs. 6 and 7 represents simulation (solid line) and analytical upper bound (dash-dotted line) BER plots of RS-coded SIMO, MISO and MIMO schemes. The close correspondence between the simulation and analytical upper bound BER results obtained for high transmit powers. The BER performance improvement from un-coded SISO to un-coded and RS-coded SIMO, MISO and MIMO schemes are given in Tables 1 and 2 respectively. The coded BER results presented in Table 2 are results obtained by simulation.

Please cite this article as: Prasad Naik R, U. Shripathi Acharya and Prabu K, High-speed and reliable Underwater Wireless Optical Communication system using Multiple-Input Multiple-Output and channel coding techniques for IoUT applications, Optics Communications (2020) 125229, https://doi.org/10.1016/j.optcom.2019.125229.

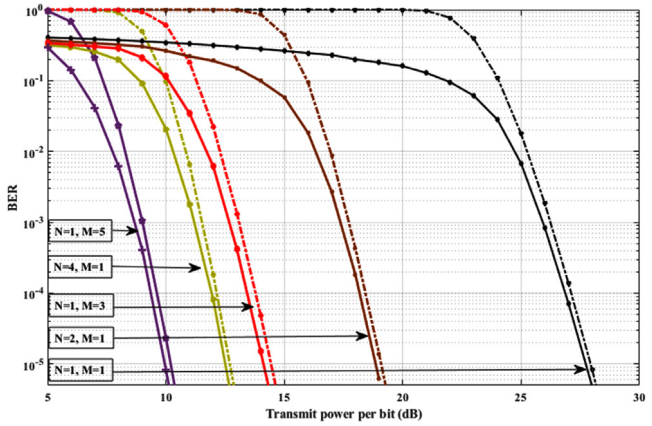

Fig. 6. Simulation and analytical BER results of RS-coded SIMO and MISO UWOC system.

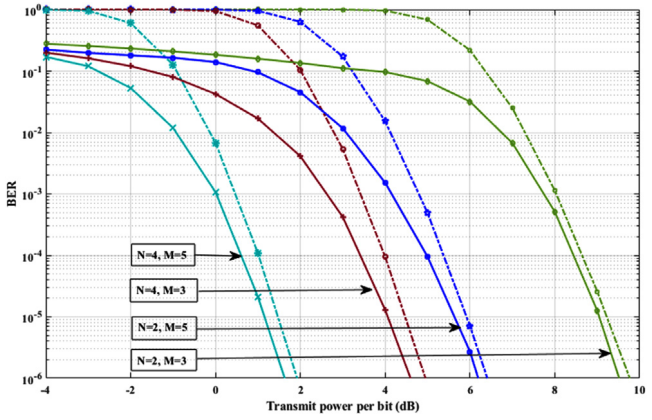

Fig. 7. Simulation and analytical BER results of $(n = 63,\ k = 51,\ t = 6)$ RS-coded MIMO UWOC system.

Table 1
Power gain comparison SIMO, MISO and MIMO schemes with respect to un-coded SISO.

Schemes	Transmit power (dB) at BER of 10^{-5}	Power gain (dB) from un-coded SISO
SISO	37.50	–
2 × 1	26.50	11.00
1 × 3	22.00	15.50
4 × 1	18.20	19.30
1 × 5	16.30	21.20
2 × 3	15.00	22.50
2 × 5	11.00	26.50
4 × 3	09.10	28.40
4 × 5	05.60	31.90

6. Conclusion

In this paper, we have analyzed the performance of the OOK modulated UWOC system employing SISO, SIMO, MISO and MIMO in the presence and absence of a channel code ((63,51) RS-code) over a channel perturbed by weak turbulence. The improvement in performance obtained by the use of MIMO and RS channel code in an UWOC system has been quantified by analysis and simulations. The proposed schemes, namely RS-coded 2 × 3, 2 × 5, 4 × 3 and 4 × 5 MIMO systems are observed to offer nearly 28, 31, 33 and 36 dB of improvement in performance (transmit power gain) respectively when compared with un-coded SISO UWOC system at BER of 10^{-5}. We conclude that the use of MIMO and diversity schemes along with suitable channel codes can be a suitable and efficient technique to realize high-speed and reliable UWOC systems. The proposed coded MIMO schemes can be gainfully used in the design of UWOC systems enabling IoUT applications such as inter submarine communication, submarine to jetty communication, communication between sensors collecting oceanic parameters and aggregating devices, etc.

Table 2
Power gain of RS-coded SIMO, MISO and MIMO techniques over un-coded SISO.

RS-coded UWOC system	Transmit Power (dB) at BER of 10^{-5}	Power gain (dB) from un-coded SISO
SISO	27.80	09.70
2 × 1	18.90	18.60
1 × 3	19.10	18.40
4 × 1	12.50	25.00
1 × 5	09.90	27.60
2 × 3	09.00	28.50
2 × 5	05.75	31.75
4 × 3	04.10	33.40
4 × 5	01.20	36.30

Table 3
a and b variation with respect to various schemes.

Scheme	N, M values	Mean and variance of normal PDF	Parameters based on calculation a'	b'	Parameters considered a	b
SISO	1, 1	−0.1647, 0.1647	0.349	2.104	0.14	3
MISO	2, 1	0.2507, 0.0959	−0.665	2.653	−1.25	3
MISO	4, 1	0.6406, 0.0525	−2.9770	5.102	−3.133	6
SIMO	1, 3	0.4815, 0.0678	−1.701	3.515	−3.150	4
SIMO	1, 5	0.7619, 0.0428	−2.977	4.102	−5.75	5
MIMO	2, 3	0.8597, 0.0362	−2.977	3.346	−5.541	5
MIMO	2, 5	1.1290, 0.0223	−6.221	5.509	−7.75	6
MIMO	4, 3	1.2237, 0.0188	−7.9139	6.45	−10.45	7
MIMO	4, 5	1.4864, 0.0114	−11.387	7.658	−13.20	8

Appendix A. Log-normal PDF using hyperbolic tangent distribution

The Cumulative Distribution Function (CDF) of normal random variable X with mean μ_X and variance σ_X^2 is,

$$\Phi(x) = \frac{1}{2} erfc\left(\frac{\mu_X - x}{\sqrt{2\sigma_X^2}}\right) \tag{22}$$

The CDF of log-normal random variable $I = \exp(2X)$ is,

$$F_I(I) = \frac{1}{2} erfc\left(\frac{2\mu_X - \ln(I)}{\sqrt{8\sigma_X^2}}\right) \tag{23}$$

From Eqs. (22) and (23), $F_I(I) = \Phi\left(\frac{\ln(I)}{2}\right)$. From [27], representation of normal CDF using the family of Hyperbolic Tangent Distribution (HTD) is given as,

$$\Phi(x) = \frac{1}{2} + \frac{1}{2}\tanh\left(b'x + a'\right) \tag{24}$$

Equating Eqs. (22) and (24), we obtain a' and b' values for particular μ_X and σ_X^2. The log-normal CDF obtained by replacing x with $\ln(I)/2$ in Eq. (24), which is given as,

$$F_I(I) = \frac{1}{2} + \frac{1}{2}\tanh\left(b'\frac{\ln(I)}{2} + a'\right) \tag{25}$$

By expanding 'tanh' into algebraic form, the CDF is obtained as $F_I(I) = \frac{\exp(2a')I^{b'}}{1+I^{b'}\exp(2a')}$, and the corresponding PDF is given as,

$$f_I(I) = \frac{b'\exp(2a')I^{b'-1}}{\left(1 + I^{b'}\exp(2a')\right)^2} \tag{26}$$

Please cite this article as: Prasad Naik R, U. Shripathi Acharya and Prabu K, High-speed and reliable Underwater Wireless Optical Communication system using Multiple-Input Multiple-Output and channel coding techniques for IoUT applications, Optics Communications (2020) 125229, https://doi.org/10.1016/j.optcom.2019.125229.

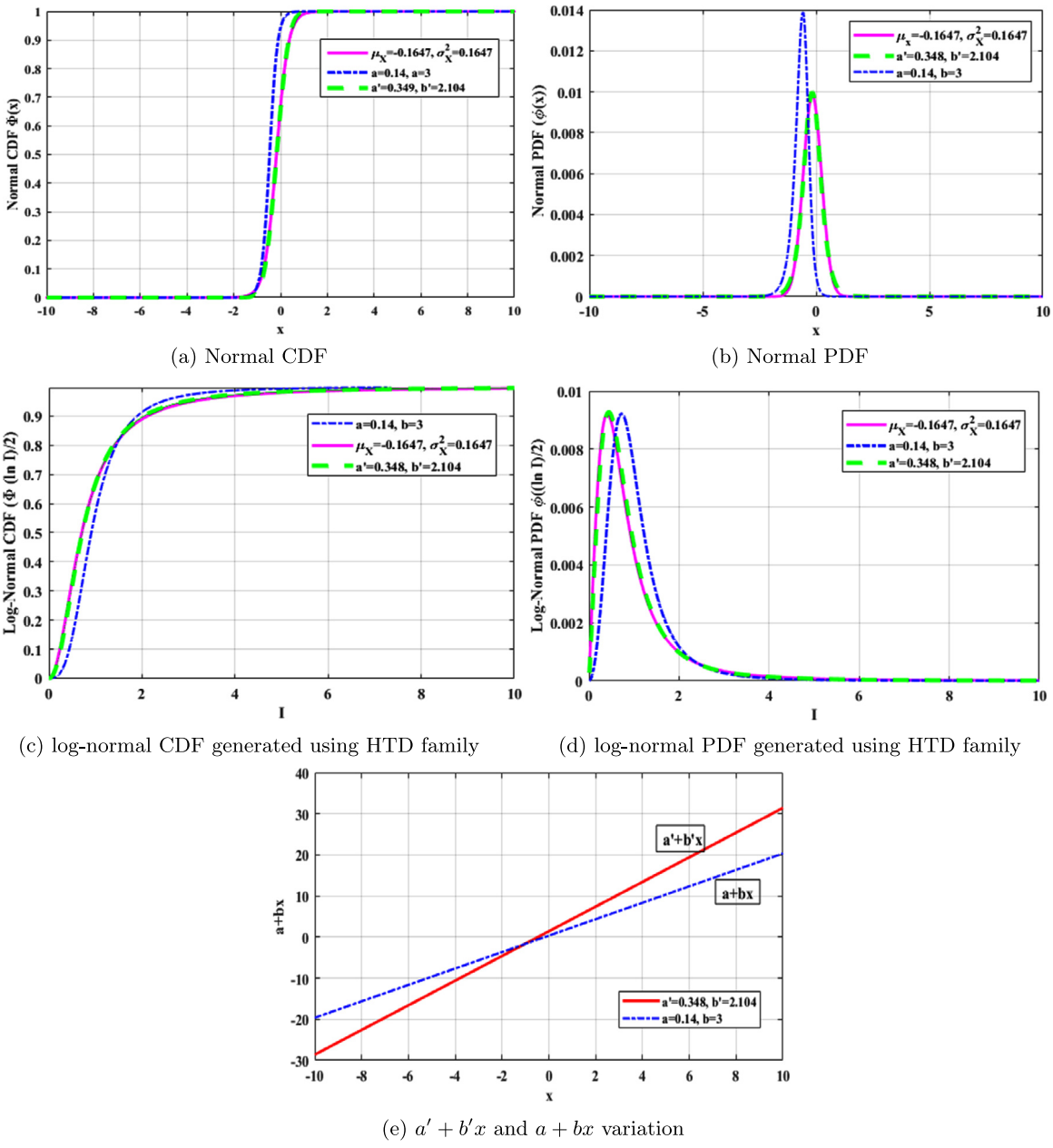

(a) Normal CDF (b) Normal PDF

(c) log-normal CDF generated using HTD family (d) log-normal PDF generated using HTD family

(e) $a' + b'x$ and $a + bx$ variation

Fig. 8. Normal and log-normal PDF and CDF.

The values of a' and b' varies based on the mean and variance of normal density function, to compute the BER (i.e, Eqs. (13), (16), (18) and (20)) 'b'' should be an integer. The PDF obtained using HTD is not guarantee that 'b'' is an integer. In our analysis, we have considered 'b' to the upper integer (floor of b' i.e, $b = \lceil b' \rceil$) and a is chosen to obtain $a + bx$ is nearest values to $a' + b'x$ for varying x. Figs. 8(a) and 8(b), represents CDF and PDF of normal random variable x generated using μ_X, σ_X^2 (solid line) and HTD (dashed line for a', b'; dashed–dotted line for a, b). Figs. 8(c) and 8(d) represents the log-normal CDF and PDF generated using HTD. Fig. 8(e) shows the variation of curves $a' + b'x$ and $a + bx$ with respect to x.

Appendix B. PDF of sum of identical, independent log-normal random variables

Let I_{sum} is sum of M independent identical log-normal random variables $(I_1, I_2, \ldots, I_M)$, i.e, $I_{sum} = I_1 + I_2 + \cdots + I_M = MI$, where $I = \exp(2X)$ log-normal random variable, X is normal random variable with mean μ_X and variance σ_X^2. From [28], I_{sum} is log-normal random variable with mean $\mathbb{E}(I_{sum}) = M\mathbb{E}(I)$ and variance $\sigma_{I_{sum}}^2 = M\sigma_I^2$, where $\sigma_I^2 = \exp(4\sigma_X^2 - 1) \times \exp(4\sigma_X^2 + 4\mu_X)$. I_{sum} can be represented in exponential form as, $I_{sum} = \exp(2U)$ then $\mathbb{E}(I_{sum}) = \exp(2\mu_U + 2\sigma_U^2)$ and $\sigma_{I_{sum}}^2 = \exp(4\sigma_U^2 + 4\mu_U)(\exp(4\sigma_U^2) - 1)$. Equating these equations, yields $\sigma_U^2 = \frac{1}{4}\ln\left(\frac{\exp(4\sigma_X^2)-1}{M} + 1\right)$ and $\mu_U = \frac{1}{2}\ln(M\mathbb{E}(I)) - \sigma_U^2$.

References

[1] M.C. Domingo, An overview of the internet of underwater things, J. Netw. Comput. Appl. 35 (6) (2012) 1879–1890.
[2] C.-C. Kao, Y.-S. Lin, G.-D. Wu, C.-J. Huang, A comprehensive study on the internet of underwater things: applications, challenges, and channel models, Sensors 17 (7) (2017) 1477.
[3] H. Kaushal, G. Kaddoum, Underwater optical wireless communication, IEEE Access 4 (2016) 1518–1547.
[4] P.N. Ramavath, A. Kumar, S.S. Godkhindi, U.S. Acharya, Experimental studies on the performance of underwater optical communication link with channel coding and interleaving, CSI Trans. ICT 6 (1) (2018) 65–70.

Please cite this article as: Prasad Naik R, U. Shripathi Acharya and Prabu K, High-speed and reliable Underwater Wireless Optical Communication system using Multiple-Input Multiple-Output and channel coding techniques for IoUT applications, Optics Communications (2020) 125229, https://doi.org/10.1016/j.optcom.2019.125229.

[5] M. Sharifzadeh, M. Ahmadirad, Performance analysis of underwater wireless optical communication systems over a wide range of optical turbulence, Opt. Commun. 427 (2018) 609–616.
[6] W. Liu, Z. Xu, L. Yang, SIMO detection schemes for underwater optical wireless communication under turbulence, Photonics Res. 3 (3) (2015) 48–53.
[7] A.C. Boucouvalas, K.P. Peppas, K. Yiannopoulos, Z. Ghassemlooy, Underwater optical wireless communications with optical amplification and spatial diversity, IEEE Photonics Technol. Lett. 28 (22) (2016) 2613–2616.
[8] M.V. Jamali, J.A. Salehi, F. Akhoundi, Performance studies of underwater wireless optical communication systems with spatial diversity: MIMO scheme, IEEE Trans. Commun. 65 (3) (2016) 1176–1192.
[9] J.A. Simpson, W.C. Cox, J.R. Krier, B. Cochenour, B.L. Hughes, J.F. Muth, 5 Mbps optical wireless communication with error correction coding for underwater sensor nodes, in: Oceans 2010 MTS/IEEE Seattle, IEEE, 2010, pp. 1–4.
[10] W.O. Popoola, Z. Ghassemlooy, J. Allen, E. Leitgeb, S. Gao, Free-space optical communication employing subcarrier modulation and spatial diversity in atmospheric turbulence channel, IET Optoelectron. 2 (1) (2008) 16–23.
[11] M.V. Jamali, J.A. Salehi, On the BER of multiple-input multiple-output underwater wireless optical communication systems, in: 2015 4th International Workshop on Optical Wireless Communications, IWOW, IEEE, 2015, pp. 26–30.
[12] H. Kaushal, G. Kaddoum, Underwater optical wireless communication, IEEE Access 4 (2016) 1518–1547.
[13] M.V. Jamali, A. Mirani, A. Parsay, B. Abolhassani, P. Nabavi, A. Chizari, P. Khorramshahi, S. Abdollahramezani, J.A. Salehi, Statistical studies of fading in underwater wireless optical channels in the presence of air bubble, temperature, and salinity random variations, IEEE Trans. Commun. 66 (10) (2018) 4706–4723.
[14] A. Tabeshnezhad, M.A. Pourmina, Outage analysis of relay-assisted underwater wireless optical communication systems, Opt. Commun. 405 (2017) 297–305.
[15] Y. Ata, Y. Baykal, Scintillations of optical plane and spherical waves in underwater turbulence, J. Opt. Soc. Amer. A 31 (7) (2014) 1552–1556.
[16] O. Korotkova, N. Farwell, E. Shchepakina, Light scintillation in oceanic turbulence, Waves Random Complex Media 22 (2) (2012) 260–266.
[17] W. Lu, L. Liu, J. Sun, Influence of temperature and salinity fluctuations on propagation behaviour of partially coherent beams in oceanic turbulence, J. Opt. A: Pure Appl. Opt. 8 (12) (2006) 1052.
[18] T.K. Moon, Error correction coding, in: Mathematical Methods and Algorithms, Jhon Wiley and Son, 2005, pp. 2001–2006.
[19] R.E. Blahut, Algebraic Codes for Data Transmission, Cambridge university press, 2003.
[20] W.O. Popoola, Z. Ghassemlooy, J. Allen, E. Leitgeb, S. Gao, Free-space optical communication employing subcarrier modulation and spatial diversity in atmospheric turbulence channel, IET Optoelectron. 2 (1) (2008) 16–23.
[21] F. Yang, J. Cheng, T.A. Tsiftsis, Free-space optical communication with nonzero boresight pointing errors, IEEE Trans. Commun. 62 (2) (2014) 713–725.
[22] M. Chiani, D. Dardari, M.K. Simon, New exponential bounds and approximations for the computation of error probability in fading channels, IEEE Trans. Wireless Commun. 2 (4) (2003) 840–845.
[23] V. Adamchik, O. Marichev, The algorithm for calculating integrals of hypergeometric type functions and its realization in REDUCE system, in: Proceedings of the International Symposium on Symbolic and Algebraic Computation, ACM, 1990, pp. 212–224.
[24] L. Fenton, The sum of log-normal probability distributions in scatter transmission systems, IRE Trans. Commun. Syst. 8 (1) (1960) 57–67.
[25] W.C. Cox, J.A. Simpson, C.P. Domizioli, J.F. Muth, B.L. Hughes, An underwater optical communication system implementing reed-solomon channel coding, in: Oceans 2008, IEEE, 2008, pp. 1–6.
[26] F. Hanson, S. Radic, High bandwidth underwater optical communication, Appl. Optics 47 (2) (2008) 277–283.
[27] A.C. Robin, A quick approximation to the normal integral, Math. Gazette 81 (490) (1997) 95–96.
[28] R.L. Mitchell, Permanence of the Log-Normal distribution, JOSA 58 (9) (1968) 1267–1272.

Please cite this article as: Prasad Naik R, U. Shripathi Acharya and Prabu K, High-speed and reliable Underwater Wireless Optical Communication system using Multiple-Input Multiple-Output and channel coding techniques for IoUT applications, Optics Communications (2020) 125229, https://doi.org/10.1016/j.optcom.2019.125229.